An image-processing based algorithm to automatically identify plant disease visual symptoms

Article *in* Biosystems Engineering · January 2009

DOI: 10.1016/j.biosystemseng.2008.09.030

2 authors:

Anyela Camargo

47 PUBLICATIONS **1,004** CITATIONS

SEE PROFILE

Jeremy Smith

University of Liverpool

137 PUBLICATIONS **1,996** CITATIONS

SEE PROFILE

Available at www.sciencedirect.com

ScienceDirect

journal homepage: www.elsevier.com/locate/issn/15375110

Research Paper: AE—Automation and Emerging Technologies

An image-processing based algorithm to automatically identify plant disease visual symptoms

A. Camargo[a,*], J.S. Smith[b]

[a]University of East Anglia, School of Computing, Norwich NR4 7TJ, England, UK
[b]Department of Electrical Engineering and Electronics, The University of Liverpool, Brownlow Hill, Liverpool L69 3GJ, UK

ARTICLE INFO

Article history:
Received 24 February 2008
Received in revised form
19 August 2008
Accepted 23 September 2008
Available online 18 November 2008

This study describes an image-processing based method that identifies the visual symptoms of plant diseases, from an analysis of coloured images. The processing algorithm developed starts by converting the RGB image of the diseased plant or leaf, into the H, I3a and I3b colour transformations. The I3a and I3b transformations are developed from a modification of the original I1I2I3 colour transformation to meet the requirements of the plant disease data set. The transformed image is then segmented by analysing the distribution of intensities in a histogram. Rather than using the traditional approach of selecting the local minimum as the threshold cut-off, the set of local maximums are located and the threshold cut-off value is determined according to their position in the histogram. This technique is particularly useful when the target in the image data set is one with a large distribution of intensities. In tests, once the image was segmented, the extracted region was post-processed to remove pixel regions not considered part of the target region. This procedure was accomplished by analysing the neighbourhood of each pixel and the gradient of change between them. To test the accuracy of the algorithm, manually segmented images were compared with those segmented automatically. Results showed that the developed algorithm was able to identify a diseased region even when that region was represented by a wide range of intensities.

1. Introduction

The emergence and development of plant diseases and pest outbreaks has become more common nowadays, as factors such as climate and environmental conditions are more unsettled than ever. The rate of spread of disease depends on current crop conditions and susceptibility to infection (Lucas et al., 1992). When plants become diseased, they can display a range of symptoms such as coloured spots, or streaks that can occur on the leaves, stems, and seeds of the plant. These visual symptoms continuously change their colour, shape and size as the disease progresses. For example Fig. 1 shows a banana leaf infected with Black Sigatoka (*Mycosphaerella fijiensis Morelet*) at various stages of infection. Fig. 1(a) shows stage 1, which is the first external symptom of the disease. It appears as a small whitish or yellow coloured spot that also resembles the first stage of the Yellow Sigatoka disease (*Mycosphaerella musicola Mulder*). These symptoms can only be observed on the underside of the leaf. In the next stage, stage 2, symptoms appear as stripes, generally brown in colour and visible on the underside of the leaf, as illustrated in Fig. 1(b). Stage 3 symptoms, Fig. 1(c), differ from stage 2 in that stripes becomes longer, wider and under certain conditions, such as with weak inoculums and unfavourable climatic conditions, can reach lengths of 20 or

* *Corresponding author.*
E-mail address: a.camargo-rodriguez@uea.ac.uk (A. Camargo).
1537-5110/$ – see front matter © 2008 IAgrE. Published by Elsevier Ltd. All rights reserved.
doi:10.1016/j.biosystemseng.2008.09.030

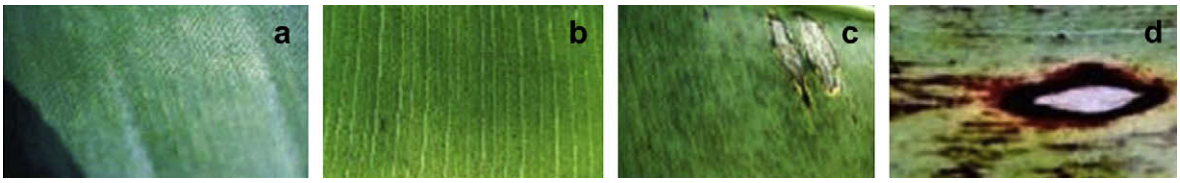

Fig. 1 – Banana leaf infected with Black Sigatoka at various stages of infection. (a) First external symptom of the disease. It appears as a small whitish or yellow coloured spot that also resembles the first stage of the Yellow Sigatoka disease; these symptoms can only be observed on the underside of the leaf; (b) symptoms appear in the shape of stripes, generally brown in colour and visible on the underside of the leaf; (c) stripes becomes longer, wider and, in certain conditions (weak inoculums and unfavourable climatic conditions), can reach a length of 2 or 3 cm; (d) the centre of the spot dries out, turns light grey, and is surrounded by a well-defined black ring which is, in turn, surrounded by a bright yellow halo. These spots remain visible after the leaf has dried out, because the ring persists (Orjeda, 1998) (courtesy of Dr Eric Fouré, CIRAD-FLHOR).

30 mm. Stage 4 symptoms, appear on the underside as a brown spot and on the upper side as a black spot. Stage 5 is when the elliptical spot is totally black and has spread to the underside of the leaf. It is surrounded by a yellow halo with the centre beginning to flatten out. In stage 6, Fig. 1(d), the centre of the spot dries out, turns light grey, and is surrounded by a well-defined black ring which is in turn surrounded by a bright yellow halo. These spots remain visible after the leaf has dried out, because the ring persists (Orjeda, 1998).

Using image-processing for disease detection has become popular in medicine, because it is a rapid and reliable way to assess a patient's condition. This practice is particularly useful when the distance between practitioner and patient prevent direct consultations. The advantage in using a 'computerised process' is the high level of accuracy in the diagnosis and prognosis, as well as the significant reduction of costs in comparison to the traditional method of face-to-face diagnosis (Dhawan, 1990). In agriculture, numerous image-processing based computerised tools have been developed to help farmers to monitor the proper growth of their crops. Special attention has been put towards the latest stages of growth, that is, when the crop is near harvesting. For example, at the time of harvesting, some computer tools are used to discriminate between plants and other objects present in the field. In the case of machines that uproot weeds, they have to discriminate between plants and weeds, whilst in the case of machines that harvest; they have to differentiate one crop from the other. Previous studies have identified the challenges and have successfully produced systems that address them (Hemming, 2000; Hemming & Rath, 2001; Philipp & Rath, 2002; Chen et al., 2002; Wang et al., 2002; Onyango, 2003). The requirements for reduced production costs, the needs of organic agriculture and the proliferation of diseases have been the driving forces for improving the quality and quantity of food production.

Thus, in the area of disease control, most research has been focused on the treatment and control of weeds, and few studies have been focused on the automatic identification of diseases. Automatic plant disease identification by visual inspection can be of great benefit to those users who have little or no information about the crop they are growing. Such users include farmers, in underdeveloped countries, who cannot afford the services of an expert agronomist, and also those living in remotes areas where access to assistance via an internet connection can become a significant factor.

This study describes an image-processing based method that identifies the visual symptoms of plant diseases from the analysis of coloured images. The algorithm starts by converting the RGB image into the H, I3a and I3b colour transformations. The I3a and I3b transformations were developed from a modification of the original I1I2I3 colour transformation, to meet the requirements of the plant disease dataset. The transformed image is then segmented by analysing the intensity distribution. Once the image was segmented, the extracted region was post-processed to remove those pixels that were not considered part of the target region. This procedure was accomplished by analysing the neighbourhood of each pixel and the gradient of change between them. To test the accuracy of the proposed

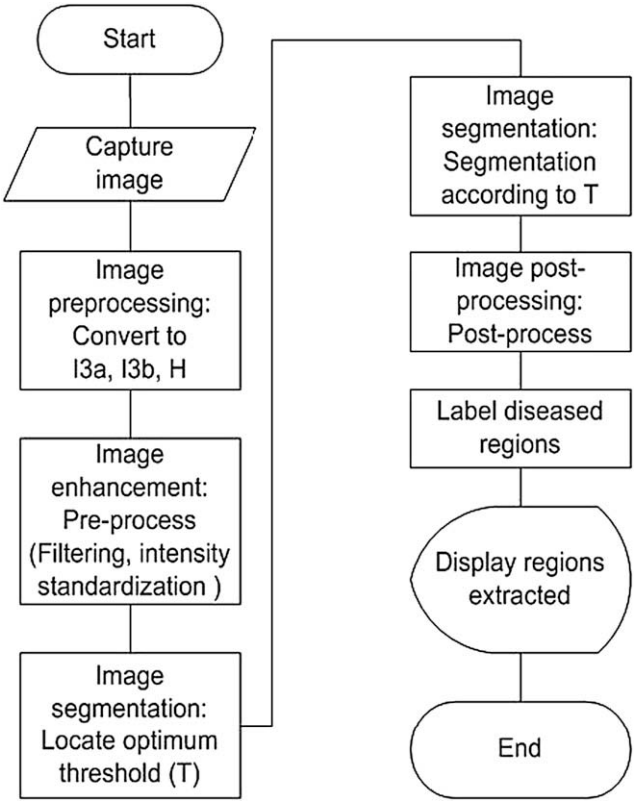

Fig. 2 – Image processing-based algorithm to automatically identify plant disease visual symptoms.

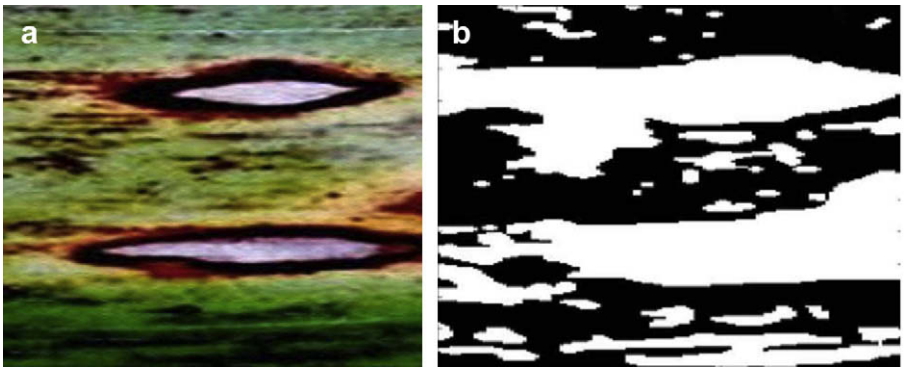

Fig. 3 – Visual disease symptom manually segmented. (a) Original image; (b) disease symptoms manually segmented.

algorithm, manually segmented image were compared with those segmented automatically.

2. Methods

This study reports on an algorithm for the detection of visual symptoms of disease by the analysis of coloured images. The algorithm was divided into four stages: (1) image pre-processing: to specify a suitable colour transformation that best highlighted the diseased regions shown in the picture; (2) image enhancement: to develop a filter that could highlight those regions considered targets (possible diseased regions); (3) image segmentation: to identify regions in the image that were likely to qualify as diseased region; (4) image post-processing: to remove unwanted background regions. A flowchart of the complete process is shown in Fig. 2.

2.1. *Image set*

The set of images used in this study were obtained from the following universities and research institutes. The International Network for the Improvement of Banana and Plantain (INIBAP, http://bananas.biodiversityinternational.org) provided a set of pictures of banana and plantain crops showing visual symptoms of different types of diseases. Some of the pictures that used the same crop were taken at different times to demonstrate disease evolution. The Department of Entomology, at the University of IOWA, USA supplied the images of maize and alfalfa. The Department of Entomology, at the University of Georgia, USA supplied the images of cotton and soya. In all cases, the image format used was JPEG, 24 bits.

2.2. *Measuring the success of the algorithm*

A testing technique was designed to determine the success of the algorithms proposed. The procedure consisted of comparing a manually segmented image, against the same image automatically segmented. In both cases, the extracted regions should have corresponded to the part of the picture showing symptoms of plant disease. The testing set was composed of 20 images corresponding to five crops, i.e. cotton, maize, banana and plantain, alfalfa and soya. To create the manually segmented set, a grid was overlaid on the image and then each box was evaluated and marked according to a colour schema; white (1) was used to represent a diseased region and black (0) used to represent a non-diseased region. The outcome of this classification was a binary image. The process was repeated for all the 20 reference images used in these test.

To evaluate the algorithm, the images were automatically segmented. The output produced was a binary image where 1 represented a pixel classified as diseased and 0 as non-diseased. To simplify the notation the manually classified set was labelled (p) and the automatically generated set (t).

Once manual and automatic sets were generated, the accuracy of the algorithm was estimated within the configuration parameters used. Using as a reference the manually segmented image, the testing consisted of two procedures that mathematically compared the two set of images (manually and automatically segmented). The comparison was carried out from two perspectives, one analysing all the pixels in the image (z), and the second analysing the pixels considered as part of the disease region (d) (Eq. (1)).

$$z = \sum_{i=1}^{m}\sum_{j=1}^{n} I(i,j);\ d = \sum_{i=1}^{m}\sum_{j=1}^{n} I(i,j) == 1 \quad (1)$$

where z represents all the pixels in the image (foreground and background) and d the diseased regions within z.

Consequently, given (d) the first test, called matching, compared the manually segmented set (p) against the automatically segmented set (t), i.e. the pixels in $p(i,j)$ equal to 1. To clarify, this, consider an image (I) of size [m (rows), n (columns)], then $I(i,j)$ represents a pixel position where ($1 \le i < m, 1 \le j < n$). Every diseased pixel in $p(i,j)$ was evaluated against $t(i,j)$. The results showed the percent of matching in t

Table 1 – Percentage misclassification and matching for the HSV and I1I2I3 colour transformations

Channel	Matching, %	Misclassified, %	av
I1	35.4	25.4	10.0
I2	58.6	24.6	34.0
I3	69.9	8.7	61.2
H	70.6	17.4	53.3
S	46.8	44.4	2.4
V	69.1	69.0	0.1

Table 2 – Segmentation according to image appearance

Image	Light			Dark		
Segmentation with channel	Matching, %	Misclassified, %	av	Matching, %	Misclassified, %	av
H	79.4	15.3	64.1	99.8	78.7	21.1
I3	34.5	24.4	10.1	69.8	12.4	57.4

given p. Ideally a perfect match would be 100% when every $d_p(i,j)$ was also in $d_t(i,j)$.

Given that p represents the manually segmented image, size $m \times n$ and t the automatically segmented image, size $m \times n$, then:

$$d_t = \sum_{i=1}^{m} \sum_{j=1}^{n} ((t(i,j)p(i,j)) == 1). \quad (2)$$

The second test compared the differences between the manual segmented and the automatically segmented images, pixel by pixel. Therefore, all the pixels in the image (z) were tested. The purpose of this test was to determine the percentage of misclassification, which is represented by Eq. (3).

$$z_t = \frac{\left(\sum_{i=1}^{m} \sum_{j=1}^{n} (t(i,j) ! = p(i,j))\right) * (m * n)}{100} \quad (3)$$

From Eqs. (2) and (3), the difference value (av) for the set of N images (i.e. 20) is Eq. (4)

$$\text{av} = (\mu d_t - \mu z)_t, \quad \text{where} \quad \mu(d_t) = \frac{\left(\sum_{\text{im}=1}^{N} d_t(\text{im})\right)}{N}, \quad \text{and} \quad \mu(z_t) = \frac{\left(\sum_{\text{im}=1}^{N} z_t(\text{im})\right)}{N} \quad (4)$$

where (im) image set and (μ) median.

The purpose of av was twofold, to compare the accuracy of the tested algorithms, and to select the best parameters involved in each algorithm.

3. Results

The testing set (shown in Annex 1) was composed of 20 images showing symptoms of plant disease in any of the five crops used in this study. As mentioned in Section 2, to create the manually segmented set of images, a grid was overlaid on the image and each position was then evaluated and marked with a colour: white (1) if the pixel resembled a disease symptom; black (0) for non-diseased regions. The outcome of this classification was a binary image. Fig. 3(a) shows one of the 20 original images and Fig. 3(b) shows the binary image produced after manual segmentation. Annex 2 shows images manually segmented; regions correspond to potential disease-affected area.

To evaluate the algorithm, original images were automatically segmented. The output produced was a binary image where again 1 represented a pixel classified as diseased and 0 as non-diseased (Annex 3).

3.1. *Colour transformation*

The purpose on this task was to find an algorithm capable of emphasizing the visual disease symptoms present in an image, with a high degree of accuracy. Part of the success in the final result was attributed to the applied colour transformations. They transformed the image to allow discrimination between diseased and non-diseased regions. Each of the transformations gave particular information about the image, i.e. those pixels representing visual disease symptoms and those representing background. At first, two colour transformations were selected: HSV (Gonzalez et al., 2004), Eq. (5), because of its ability to deal with varying lighting conditions, and I1I2I3 (Ohta et al., 1980), because a previous study (Philipp & Rath, 2002) showed that this method worked well when tested on pictures of plants.

Given that (I) exists in the RGB colour space, then:

$$\text{mx}_{(i,j)} = \max\left(I_{R(i,j)}, I_{G(i,j)}, I_{B(i,j)}\right); \quad \min_{(i,j)} = \min\left(I_{R(i,j)}, I_{G(i,j)}, I_{B(i,j)}\right)$$

$$H(i,j) = \begin{pmatrix} \frac{60*\left(I_{G(i,j)} - I_{B(i,j)}\right)}{\text{mx}-\min} & I_{R(i,j)} > \max\left(I_{G(i,j)}, I_{B(i,j)}\right) \\ \frac{180*\left(I_{B(i,j)} - I_{R(i,j)}\right)}{\text{mx}-\min} & I_{G(i,j)} > \max\left(I_{R(i,j)}, I_{B(i,j)}\right) \\ \frac{300*\left(I_{R(i,j)} - I_{G(i,j)}\right)}{\text{mx}-\min} & I_{B(i,j)} > \max\left(I_{R(i,j)}, I_{G(i,j)}\right) \end{pmatrix} \quad (5)$$

$$S(i,j) = \left[\frac{\text{mx} - \min}{\text{mx}}\right]$$

$$V(i,j) = [\text{mx}]$$

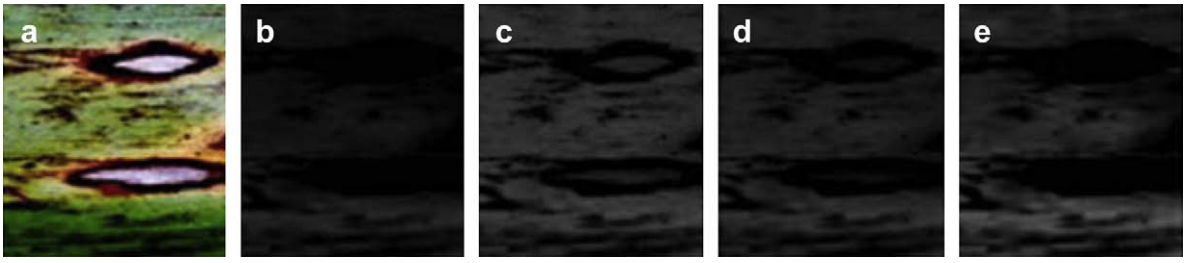

Fig. 4 – Regions discrimination when varying *m* and de in I3 channel. (a) Original image; (b) *m* = 2, de = 4; (c) *m* = 3, de = 4; (d) *m* = 2.5, de = 4; (e) *m* = 2, de = 2.

Table 3 – Evaluating the best *m* and de values. (a) de = 4, varying *m* (b) *m* = 2, varying de

m	Matching, %	Misclassified, %	av	de	Matching, %	Misclassified, %	av
(a) de = 4				(b) *m* = 2			
0.5	51.2	35.4	15.8	0.5	64.4	9.7	54.8
1	60.1	23.6	36.5	1	67.6	9.7	57.9
1.5	64.3	19.2	45.1	1.5	67.8	9.6	58.2
2	78.2	13.3	64.9	2	68.1	9.7	58.4
2.5	87.5	19.5	68.0	2.5	67.7	9.8	57.9
3	82.7	28.9	53.8	3	63.4	9.6	53.8
3.5	89.1	33.1	56.0	3.5	65.2	10.0	55.2
4	90.2	39.6	50.7	2	78.2	13.3	64.9
4.5	87.1	40.1	47.0	4.5	65.3	9.6	55.7
5	83.5	39.4	44.1	5	50.1	8.5	41.6

Eq. (6) shows how the I1I2I3 colour transformations are calculated.

$$I_1 = \left(I_{R(i,j)} + I_{G(i,j)} + I_{B(i,j)}\right)/3$$

$$I_2 = \left(I_{R(i,j)} - I_{B(i,j)}\right)/2 \tag{6}$$

$$I_3 = \left(\left(2 * I_{G(i,j)}\right) \sum I_{R(i,j)} \sum I_{B(i,j)}\right)/4$$

where $0 \leq I_R, I_G, I_B \leq 255$.

These two schemes were tested to determine the selection of the colour transformation(s) that best highlighted the possible diseased regions in the image. Using visual inspection, before any numerical analysis, I3 and H appeared to show better region discrimination. The numerical results of the tests confirmed this. For instance, Table 1 shows that I3, in comparison with the other transformations, achieves good pixel matching (69.9%) and obtained the lowest level of misclassification (8.7%). Notice also that although V achieved the third highest rate of pixel classification (69.1%), the rate of pixels that were incorrectly classified was also high (69.0%).

Table 1 presents the averaged results for all 20 images. The results gave sufficient reason to discard the I1, S and V colour transformations. As for I2, its av rate is higher in comparison with the lowest values, yet it is still far from the 50% accuracy that was considered to be the cut-off threshold.

The results of this test led to the selection of the I3 and H colour transformations. It had been anticipated that both the I3 and H transformations would be used for segmentation, as in circumstances where the disease is rather "light" in appearance (e.g. Annex 1 (17)) it cannot be well-defined by I3, but can be detected by H. Table 2 shows the effects of having segmented a set of light images with the H channel (15.30% misclassification) and with the I3 channel (24.4% misclassification). The same pattern is repeated with dark images (e.g. Annex 1 (1)) when segmenting using the H channel (78.7% misclassification). Note that the loss of information is especially important when light colour images are segmented. Therefore, to identify the most appropriate transformation, an analysis of the intensity distribution of the image should be made before segmentation is attempted.

Despite I3 providing the best performance in relation to matching/misclassification, the results were not completely accurate. The rate of misclassified pixels was still an issue to be tackled and for that reason I3 was modified as explained in the following section.

3.1.1. *Selecting parameters for I3*

Two different tests were undertaken on arbitrary disease regions, in order to select the appropriate values for the I3 colour transformation. To facilitate the manipulation of I3, consider Eq. (7):

From Eq. (6)

$$I_3 = \left(\left(m * I_{G(i,j)}\right) - I_{R(i,j)} - I_{B(i,j)}\right)/\mathrm{de} \tag{7}$$

where *m* and de are the values to be optimized.

The first test consisted of keeping de constant and varying *m*, the value of *m* was modified as a result of observing the transformed images. The results of this manual test determined that *m* should be approximately 2.5, as when *m* was

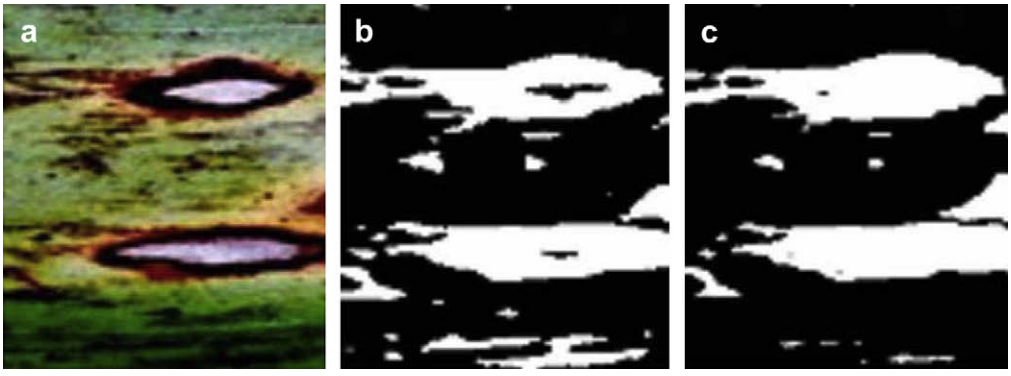

Fig. 5 – I3a and I3b image region discrimination. (a) Original image; (b) I3a *m* = 2.5, de = 4; (c) I3b, *m* = 2, *de* = 2.

Table 4 – Comparing the different outputs when varying [σ, k] in the Gaussian filter. (a) $k = 4$, varying σ; (b) $\sigma = 0.9$, varying k

σ	Matching, %	Misclassified, %	av	k	Matching, %	Misclassified, %	av
(a) $k = 4$				(b) $\sigma = 0.4$			
0.4	80.2	9.3	71.0	3	76.7	9.9	66.8
0.8	79.9	13.4	66.5	4	84.5	8.2	76.3
0.9	84.5	8.2	76.3	5	85.2	10.0	75.1
1.2	80.2	8.4	71.8	6	83.7	9.7	74.0
1.6	80.0	8.7	71.3	7	75.2	11.1	64.1
				8	81.0	13.0	68.1

increased above this value, the diseased regions with lighter intensities would be easily mixed up with regions representing background. Fig. 4(a) is the original image that was segmented several times, with Eq. (7), in order to find the best values for m and de. Fig. 4(b) shows the segmented image when applying the original I3 equation. Clearly, there is no difference between the potential regions. Fig. 4(c) is an example of what happens when the multiply parameter (m) is increased to 3; the inner regions within the spots resemble the intensities that correspond to that which enclose the background. On the contrary, with de = 2.5 and $m = 4$ (Fig. 4(d)) the diseased regions are much better detected in comparison to the two previous trials. Fig. 4(e) with de = 2 and $m = 2$ also shows an image whose background and foreground regions are subtly defined.

The second test used the matching and misclassification analysis to validate the results estimated by visual inspection. The test quantified the results of the visual inspection, shown in Table 3(a). For example, I3a obtained the best matching/misclassification factor (67.9%), when de and m parameters were set to 4 and 2, respectively. On the contrary, the lowest av factor (44.1%) was obtained when $m = 5$. To select the best parameters of I3b, a similar testing procedure was performed: the results are shown in Table 3(b). According to these results, the best (58.4%) was obtained when de = 2. However, the complete distribution was very tight, as the second best av factor (58.2%) was obtained when de = 1.5.

As a result of the testing scheme carried out to select the m and de values for the I3 equation, the following two equations were developed.

$$I_3a = ((2.5 * I_G(i,j)) - I_R(i,j) - I_B(i,j))/4 \quad (8)$$

$$I_3b = ((2 * I_G(i,j)) - I_R(i,j) - I_B(i,j))/2 \quad (9)$$

Another highlight of these experiments was the fact that I3a and I3b were complementary. I3a is capable of segmenting the majority of information regarding a visual disease symptom. This is demonstrated by Fig. 5(a) which shows the original picture, and Fig. 5(b), which shows the diseased regions segmented with I3a. However, when the disease region includes light or pale zones, they can be better detected and segmented using I3b, as shown in Fig. 5(c).

3.2. *Pre-processing*

The previous stage looked for a suitable colour transformation capable of coping with the requirements of the plant disease image data set. The objective of pre-processing is to adjust the intensities of the image in order to highlight areas considered as targets (visual symptoms of disease). After this process the image will be ready for segmentation.

3.2.1. *Image enhancement*

The objective of image enhancement is to improve the quality of the image by different means e.g. varying intensities, so that segmentation can be more efficient. Therefore, success in the segmentation process is determined by the accuracy with which diseased regions of the image were correctly selected. To begin the process, images were enhanced by means of applying a Gaussian filter. This filter suppresses high frequencies; its effect is to blur the image, in a similar manner to the mean filter. The degree of smoothing is determined by the standard deviation (σ) of the associated probability distribution, Eq. (10).

$$G(i,j) = I_0(i,j) * e^{\left(-\frac{i^2+j^2}{2\sigma * (i,j)}\right)} \quad (10)$$

in the Gaussian filter equation, the parameter σ has to be proportional to the size of the neighbourhood (convolution matrix) on which the filter operates (Sonka et al., 1999). In anticipation that a larger (σ) leads to a larger convolution matrix (k), an initial trial was undertaken to roughly

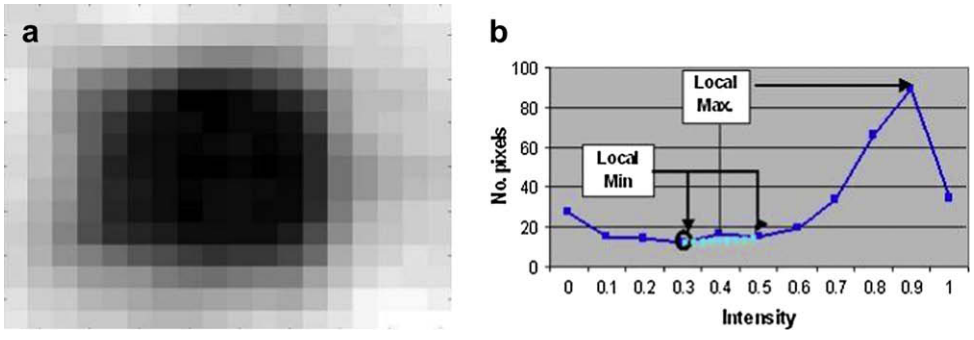

Fig. 6 – Image histogram. (a) Original image, Annex 1, Image 1. (b) Histogram of intensities interval [0,1].

Table 5 – Segmentation with different number of bins in the histogram

Distance between bins	Bins	Matching, %	Misclassified, %	av
0.025	41	80.4	11.8	68.6
0.015	67	75.3	10.8	64.5
0.01	101	84.5	8.2	76.2
0.007	143	83.4	8.0	75.4
0.005	201	81.9	7.9	74.0
0.0025	401	84.5	8.2	76.3
0.001	1001	85.6	8.5	77.1
0.00025	40001	83.4	9.4	74.0

determine the values of (σ) and (k). Initially k was varied within the range [3–8], and (σ) within the interval [0–2], with values increasing at a rate of 0.1. Once the image was filtered, the standard deviations of the eigenvectors were calculated and compared. One conclusion to be drawn from the results obtained was that σ should not be greater than 1, because above this value no significant effects were produced in the image and that, at all times, k set to 4 was the most appropriate combination with σ.

The values of (σ) and (k) were varied in accordance with the first test, matching and the misclassification percentages were then determined. Table 4(a) shows that with $k = 4$ the best av results were obtained at $\sigma = 0.9$ (75.8%), whereas Table 4(b) shows that with $\sigma = 0.9$ and varying k, the optimum value was obtained at $k = 4$ (76.3%).

After using the I3a transformation and applying the filter, the interval of the image intensity varied between -1 and 1 for some images. For other images, the interval varied from 0 to 1, or from 0 to 0.1. To overcome this problem, the resulting image was normalized within the interval [0, 1].

3.3. *Image segmentation*

Once the image was both enhanced and normalized, the next procedure was to identify an optimum threshold that could differentiate between background and target object (i.e. the region showing the current symptoms of the disease). Following the investigation of a number of segmentation techniques the ''histogram of intensities'' was selected (Prewitt, 1970). This section explains how diseased and background regions were separated. The segmentation procedure was undertaken using a threshold value that was calculated applying segmentation by maximum intensity location in a histogram of frequencies. The idea of this procedure is to accurately interpret the distribution of the data along the histogram, so that the appropriate threshold point can be easily identified. Mathematically speaking, the histogram is denoted as $y_0, y_1, \ldots, y_n$ where y_i is the number of pixels in the image (I) with grey level i, and n is the maximum grey level attained (Glasbey, 1993). When analysing the distribution, usually the highest peak ($h(y_i)$) represents a common range of intensities within the image, whilst intensities with low values in between two greater neighbours could represent an edge. This is illustrated in Fig. 6, where Fig. 6(a) represents the image and Fig. 6(b) the associated histogram. The threshold is the local minimum (Fig. 6(b)), which represents an evident change in the intensity values of the regions analysed.

This study used the theory previously described. However, the method to select the threshold value was modified because of the characteristics of the data set of images. In essence, the distribution of image intensities was more complex. For example, as the highest peak did not always represent an undesired region, an alternative approach was used to identify optimal number of bins in the histogram, as well as the optimal cut-off threshold. To identify the optimal number of bins, the distribution of image intensity was plotted into different intervals, such as [0:0.025:1] 41 bins, [0:0.01:1] 101 bins, [0:0.001:1] 1001 bins and [0:0.00025:1] 40001 bins. Then the data set of images was tested to compare the matching/misclassification performance when using different ranges of bins. Results of the test suggested that the interval [0:0.001:1] offered the best results in comparison to the others. Table 5 shows the results obtained when the image dataset was segmented using different number of bins in the histogram of intensities.

To investigate the most appropriate threshold method the following procedure was undertaken:

- The mean ($\mu = \sum \mathrm{I3a}(i,j)/m*n$) and standard deviation ($\sigma(\mathrm{I3a})$) of the colour transformation were calculated, the standard deviation gave the variability of the distribution.
- The mean (μ) and standard deviation (σ) gave the limits of the distribution within which the threshold value would be calculated. That is to say, all the pixels $I(i,j)$ whose intensities were as far as one standard deviation from the mean could count as a potential threshold point (pT), i.e. $\mathrm{pT} = [\mu(\mathrm{I3a}) - \sigma(\mathrm{I3a})]$. This is represented mathematically in Eq. (11):

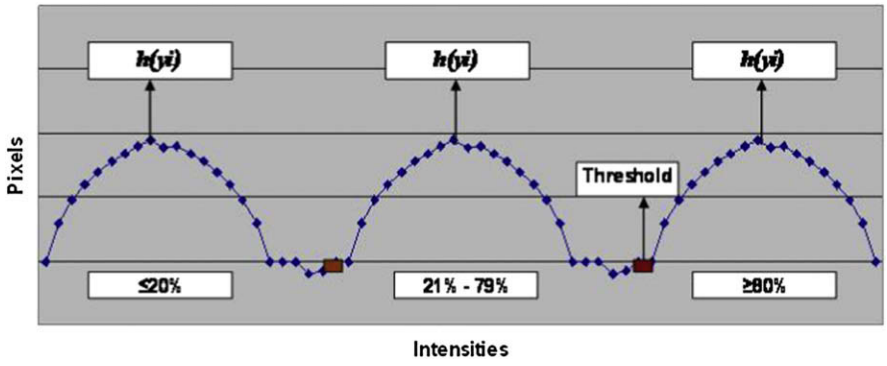

Fig. 7 – Method used to location of global local maximum $h(y_i)$.

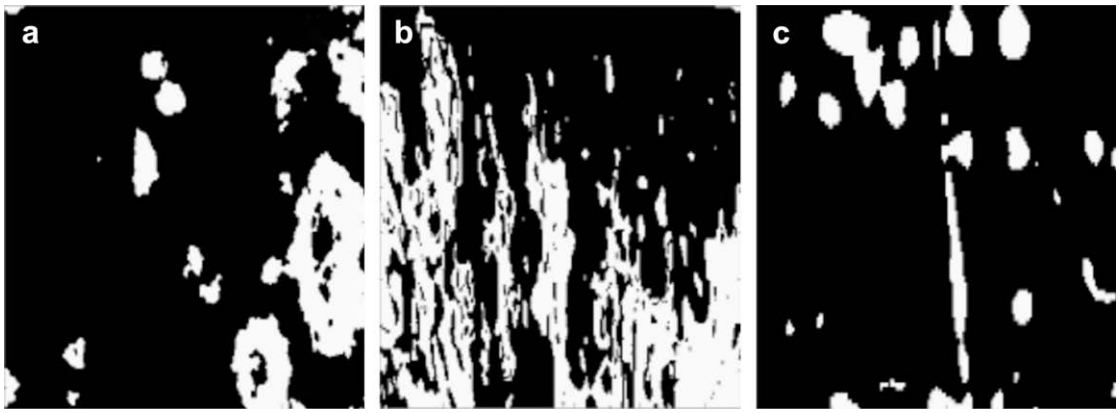

Fig. 8 – Results of automatic image segmentation. (a) Annex 1, Image 3, (b) Annex 1, Image 7 (c) Annex 1, Image 17.

$$I(i,j) \subset (\mathrm{I3a}(i,j) \geq \mathrm{pT}) \tag{11}$$

- Similarly, the global local maximum I3a($h(y_i)$) was located in the histogram. According to its position (Fig. 7), this was classified as being either in the first 20% of the distribution, the last 80%, or between 21 and 79%. Fig. 8(a) and (b) shows the results from three of the most difficult to analyse images. Each original image has high variability in terms of intensity, additionally, every spot is different in colour and shape and the inner region does not resemble the outer area.

This procedure was repeated with the I3b and H colour transformations.

Regarding $h(y_i)$'s I3a, I3b and H positions, these three segmented images were summed up in order to get a unified one of the form I3a + I3b + H. However, there were some exceptions, for example in images with the characteristics of Annex 1 (17), with light spots enclosed in dark backgrounds. Commonly the H's local maximum is located at the very end of the distribution, somewhere above 80%. In that case, the selection of a unique channel (H) was enough to extract the major number of pixels that corresponded to diseased regions. Fig. 8(c) shows the final image after segmentation.

Another exception occurs when the cut-off threshold point was of a value less than 0 (pT < 0). The final matrix could then be the matrix result of what was obtained when segmenting the I3b channel (Table 6). Fig. 8(a) and (b) shows the result of three images. Each original has high variability in terms of intensity, with every spot differing in colour and shape and the inner regions not resembling the outer. The common characteristic of these two images was that they had dark spots enclosed in dark backgrounds, for which the final matrix was most likely to be the sum of I3a + I3b + H. On the contrary, Fig. 8(c) is an example of light spots on a dark background, for which the location of ($h(y_i)$) is most likely to be somewhere beyond 80%. In this case, the final matrix is the result of what is obtained by segmenting the H channel.

3.4. *Post-processing*

Apart from the two exceptions mentioned above, the segmentation process produced three matrices corresponding to the I3a, I3b and H channels. Each matrix contained the regions that, according to the analysis undertaken in the previous section, could be disease symptoms. These three matrices were summed and turned into a unique matrix, which represents the set of diseased regions (Fig. 9). Since the summed matrix still contains regions of pixels either too small or unconnected, the small regions of pixels were deleted using the morphological binary open function, which removes all connected regions that have fewer than P (six for this experiment) pixels. Another procedure filled holes using region filling. These two methods are part of the mathematical morphology operations.

Fig. 10(a) and (b) presents the resulting images after the segmentation and post-processing procedures. The most relevant regions in terms of area having been selected, labelling is applied then to classify each region. Fig. 10(b) shows the extracted image with a number of potentially diseased regions. To demonstrate the success of the process, the original region was placed under the final segmented regions.

3.5. *Assessing segmentation accuracy*

To demonstrate the accuracy of the algorithm, the same 20 images, used during the process of image segmentation, were tested again. The results are shown in Table 7. Annex 1 contains the original images; Annex 3 shows the results from trials on these images. Fig. 10(b) is the result of an image segmented with the algorithm proposed. Note that the algorithm proposed was able to identify diseased regions in most of the images tested. For example, image no. 7 was one of the most difficult to analyse because of the wide range of intensities that embraced its diseased region. However, the automatically segmented image shows those specific regions that were considered diseased regions.

Table 6 – Output according ($h(y_i)$) [I3a,I3b,H] positions

Final matrix	$h(y_i)$ location		
	≤20%	21–79%	≥80%
H	I3a, I3b	I3a, I3b	H
I3b	T < 0		
I3a + I3b + H	I3a, I3b, H	I3a, I3b, H	I3a, I3b, H

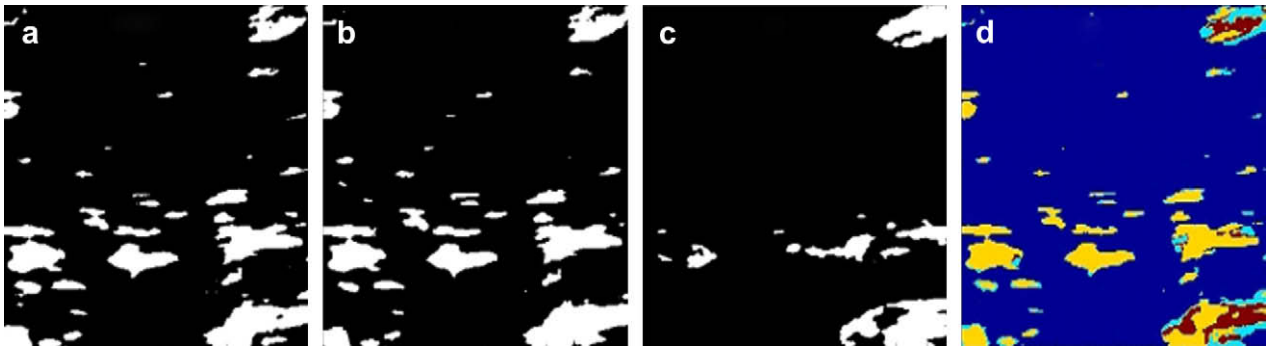

Fig. 9 – Image output for I3a, I3b, and H channel. Original, image 5. (a) I3a channel; (b) I3b channel; (c) H channel; (d) I3a + I3b + H channels.

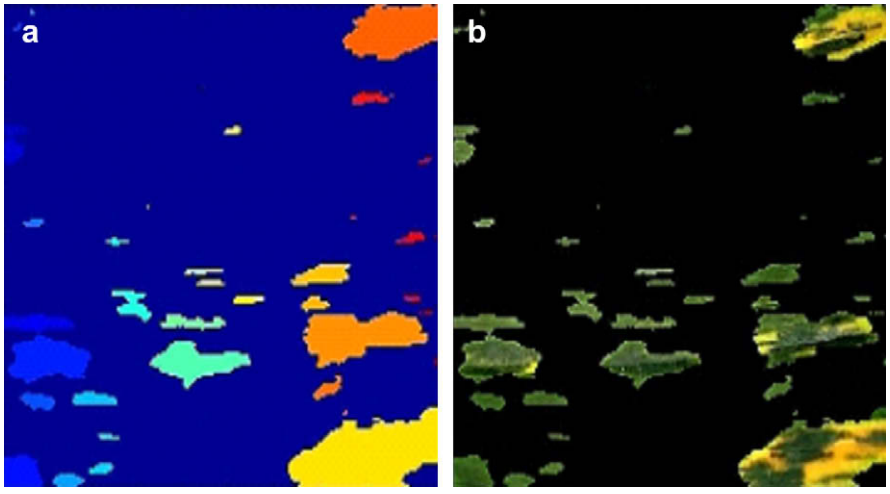

Fig. 10 – Image post-processing. Original Annex 1, Image 5. (a) Diseased regions; (b) final image with original intensities.

4. Conclusions

The strategy for image segmentation described effectively detects and selects the regions that, from the point of view of a human expert, are considered diseased. The strength of this algorithm is the ability to identify the correct target (diseased region) in images with different range of intensities distribution. To justify this statement, the algorithm was tested on a very diverse set of images and segmentation performance was estimated. Because of the complexity of the images used in this study, the strategy proposed here may be suitable for other type of images whose targets are different to that of images showing diseased plants. The next stage of developing a disease classification system is to extract parameters of the diseased region and classify the image accordingly.

Acknowledgement

The authors wish to give thanks to INIBAP, especially Dr Eric Fouré, CIRAD-FLHOR, for the information they kindly provided to this research. They would also like to thanks the Departments of Entomology at the universities of Iowa and Georgia for producing and provided the test images used in this research.

Table 7 – Segmentation algorithm, final results showing percent of matching and misclassification

Image	Matching, %	Misclassified, %	av	Diseased pixels, %
1	95.6	4.6	91	3.1
2	72.4	11.7	60.7	12.3
3	67.2	8.1	59.1	21.6
4	96.5	13.9	82.6	7.3
5	42	18.6	23.4	31.4
6	56.3	15.1	41.2	34.1
7	48.7	35.5	13.2	68.8
8	59.3	20.6	38.7	46.2
9	85	4.7	80.3	6.2
10	85.2	11	74.2	7.9
11	65.6	15.2	50.4	41.6
12	61.2	15.3	45.9	24
13	64.4	24.9	39.5	20.4
14	77.6	10	67.6	40.9
15	86.5	6.2	80.3	32.6
16	85.9	4.5	81.4	12.1
17	94.4	5.7	88.7	4.6
18	95.9	2.2	93.7	7.4
19	98.3	3.8	94.5	11.1
20	93	6.4	86.6	10.5

Appendix.


(1) Cotton: southern green stink bug (*Nezara viridula*)


(2) Cotton: Ascochyta blight of cotton (*Ascochyta gossypii*)


(3) Cotton: Ascochyta blight of cotton (*Ascochyta gossypii*)


(4) Cotton: bacterial angular leaf spot of cotton (*Xanthomonas campestris*)


(5) Banana: black Sigatoka


(6) Banana: Eumusae leaf spot disease (*Mycosphaerella eumusae*)


(7) Banana: Black leaf streak disease (*Mycosphaerella fijiensis*)


(8) Banana: Sigatoka disease (*Mycosphaerella musicola*)


(9) Alfalfa: Leptosphaerulina leaf spot.


(10) Alfalfa: Leptosphaerulina leaf spot.


(11) Corn: brown spot of corn (*Physoderma maydis*)


(12) Corn: maize dwarf mosaic virus


(13) Corn: Southern corn leaf blight and stalk rot (*Helminthosporium maydis*)


(14) Corn: Southern corn leaf blight and stalk rot (*Helminthosporium maydis*)


(15) Corn: Anthracnose leaf blight


(16) Soya: Bacterial blight (*Pseudomonas syringae*)


(17) Soya: downy mildew (*Peronospora manshurica*)


(18) Soya: frogeye leaf spot (*Cercospora sojina*)


(19) Soya: Cotton, Ascochyta blight of cotton (*Ascochyta gossypii*)


(20) Alfalfa: Leptosphaerulina leaf spot.

Annex 1

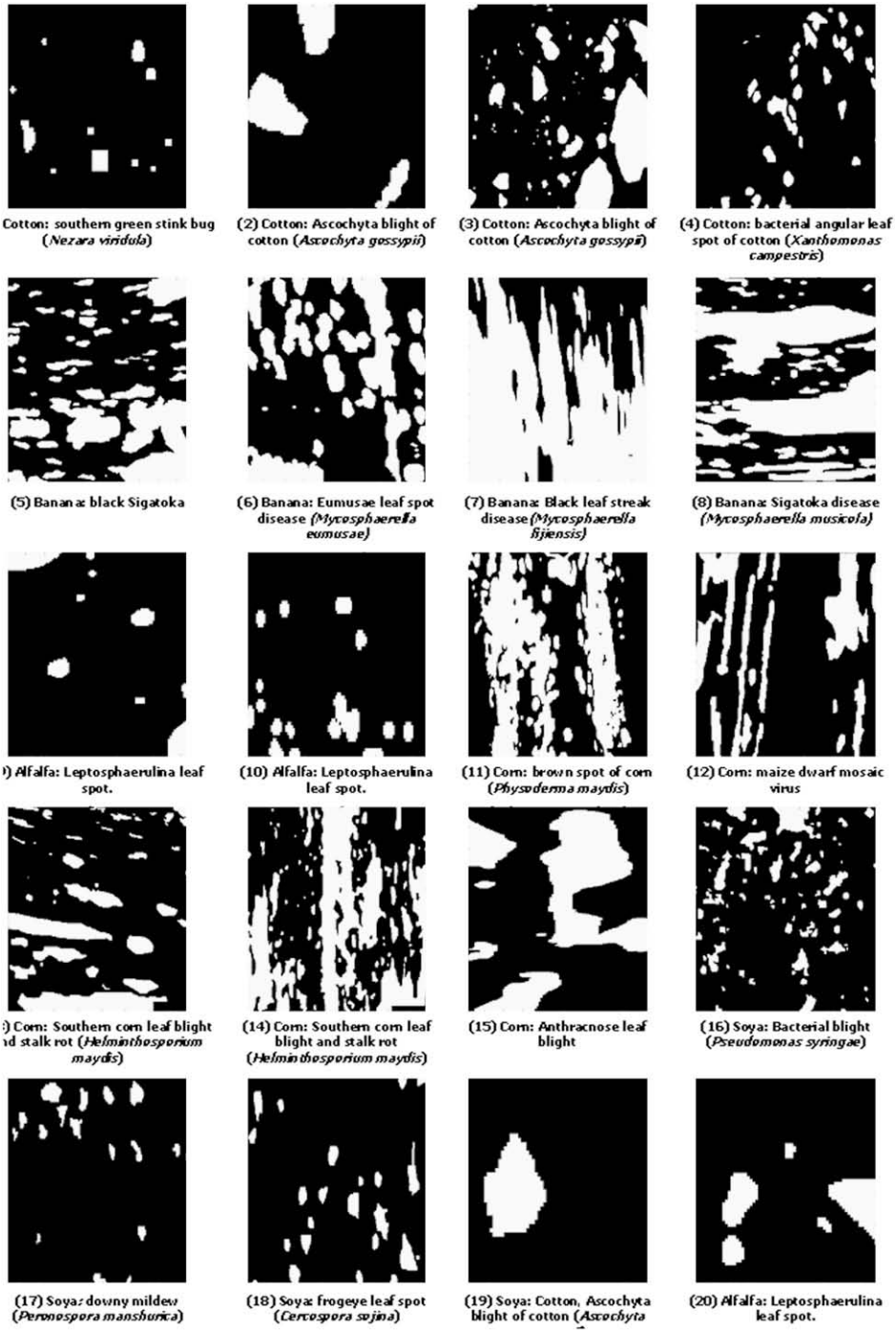
Cotton: southern green stink bug (*Nezara viridula*)
(2) Cotton: Ascochyta blight of cotton (*Ascochyta gossypii*)
(3) Cotton: Ascochyta blight of cotton (*Ascochyta gossypii*)
(4) Cotton: bacterial angular leaf spot of cotton (*Xanthomonas campestris*)
(5) Banana: black Sigatoka
(6) Banana: Eumusae leaf spot disease (*Mycosphaerella eumusae*)
(7) Banana: Black leaf streak disease (*Mycosphaerella fijiensis*)
(8) Banana: Sigatoka disease (*Mycosphaerella musicola*)
) Alfalfa: Leptosphaerulina leaf spot.
(10) Alfalfa: Leptosphaerulina leaf spot.
(11) Corn: brown spot of corn (*Physoderma maydis*)
(12) Corn: maize dwarf mosaic virus
) Corn: Southern corn leaf blight id stalk rot (*Helminthosporium maydis*)
(14) Corn: Southern corn leaf blight and stalk rot (*Helminthosporium maydis*)
(15) Corn: Anthracnose leaf blight
(16) Soya: Bacterial blight (*Pseudomonas syringae*)
(17) Soya: downy mildew (*Peronospora manshurica*)
(18) Soya: frogeye leaf spot (*Cercospora sojina*)
(19) Soya: Cotton, Ascochyta blight of cotton (*Ascochyta*
(20) Alfalfa: Leptosphaerulina leaf spot.

Annex 2

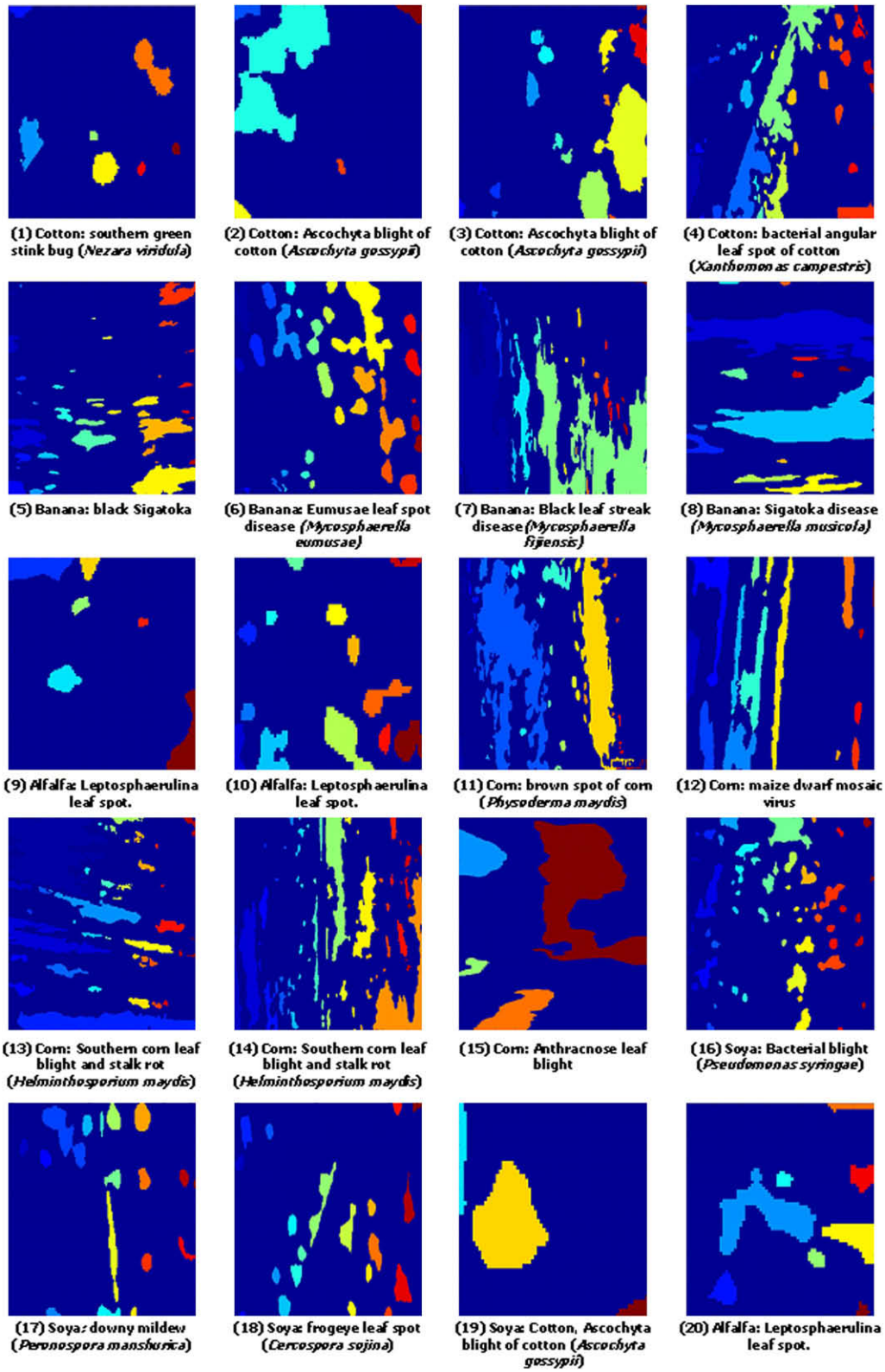
(1) Cotton: southern green stink bug (*Nezara viridula*)
(2) Cotton: Ascochyta blight of cotton (*Ascochyta gossypii*)
(3) Cotton: Ascochyta blight of cotton (*Ascochyta gossypii*)
(4) Cotton: bacterial angular leaf spot of cotton (*Xanthomonas campestris*)
(5) Banana: black Sigatoka
(6) Banana: Eumusae leaf spot disease (*Mycosphaerella eumusae*)
(7) Banana: Black leaf streak disease (*Mycosphaerella fijiensis*)
(8) Banana: Sigatoka disease (*Mycosphaerella musicola*)
(9) Alfalfa: Leptosphaerulina leaf spot.
(10) Alfalfa: Leptosphaerulina leaf spot.
(11) Corn: brown spot of corn (*Physoderma maydis*)
(12) Corn: maize dwarf mosaic virus
(13) Corn: Southern corn leaf blight and stalk rot (*Helminthosporium maydis*)
(14) Corn: Southern corn leaf blight and stalk rot (*Helminthosporium maydis*)
(15) Corn: Anthracnose leaf blight
(16) Soya: Bacterial blight (*Pseudomonas syringae*)
(17) Soya: downy mildew (*Peronospora manshurica*)
(18) Soya: frogeye leaf spot (*Cercospora sojina*)
(19) Soya: Cotton, Ascochyta blight of cotton (*Ascochyta gossypii*)
(20) Alfalfa: Leptosphaerulina leaf spot.

Annex 3

REFERENCES

Chen Y R; Chao K; Moon S K (2002). Machine vision technology for agricultural applications. Computers and Electronics in Agriculture, **36**(2–3), 173–191.

Dhawan A P (1990). A review on biomedical image processing and future trends. Computer Methods and Programs in Biomedicine, **31**(3–4 SU), 141–183.

Glasbey C A (1993). An analysis of histogram-based thresholding algorithms. Graphical Models and Image Processing, **55**(6), 532–537.

Gonzalez R C; Woods R E; Eddins S L (2004). Digital Image Processing Using MATLAB. Prentice Hall.

Hemming J (2000)Computer Vision for Identifying Weeds in Crops. Gartenbautechnische Informationen, **Heft 50**. Institut fur Technick in Gartenbau und Landwirtschaft, Universität Hannover.

Hemming J; Rath T (2001). Computer-vision-based weed identification under field conditions using controlled lighting. Journal of Agricultural Engineering, **78**(3), 233–243.

Lucas B G; Campbell C L; Lucas L T (1992). Introduction to Plant Diseases: Identification and Management. Van Nostrand Reinhold, U.S.

Ohta Y U; Kanade T; Sakai T (1980). Color information for region segmentation. Computer Graphics and Image Processing, **13**, 222–241.

Onyango C M (2003). Segmentation of row crop plants from weeds using colour and morphology. Computers and Electronics in Agriculture, **39**, 141–155.

Orjeda G (1998). Evaluation of Musa germplasm for resistance to Sigatoka diseases and Fusarium wilt. INIBAP Technical Guidelines, 3. International Plant Genetic Resources Institute, Rome, Italy; International Network for the Improvement of Banana and Plantain, Montpellier, France; ACP-EU Technical Centre for Agricultural and Rural Cooperation, Wageningen, The Netherlands.

Philipp I; Rath T (2002). Improving plant discrimination in image processing by use of different colour space transformations. Computers and Electronics in Agriculture, **35**(1), 1–15.

Prewitt J (1970). Object enhancement and extraction. In Picture Processing and Psychopictorics. Academic Press, New York.

Sonka M; Hlavac V; Boyle R (1999). Image Processing, Analysis, and Machine Vision (second ed.). PWS Publishing, Pacific Grove, CA.

Wang D; Ram M S; Dowell F E (2002). Classification of damaged soybean seeds using near-infrared spectroscopy. American Society of Agricultural Engineers, **4**(6), 1943–1948.